Environmental Science and Ecotechnology 14 (2023) 100228

Contents lists available at ScienceDirect

Environmental Science and Ecotechnology

journal homepage: www.journals.elsevier.com/environmental-science-and-ecotechnology/

Original Research

Global methyl halide emissions from biomass burning during 2003–2021

Xiaoyi Hu [a], Di Chen [a], Liting Hu [a], Bowei Li [a], Xinhe Li [a], Xuekun Fang [a, b, c, *]

[a] College of Environmental & Resource Sciences, Zhejiang University, Hangzhou, Zhejiang, 310058, PR China
[b] State Key Joint Laboratory for Environmental Simulation and Pollution Control, College of Environmental Sciences and Engineering, Peking University, Beijing, 100871, PR China
[c] Center for Global Change Science, Massachusetts Institute of Technology, Cambridge, MA, 02139, USA

ARTICLE INFO

Article history:
Received 3 August 2022
Received in revised form
24 November 2022
Accepted 24 November 2022

Keywords:
Methyl halides
Biomass burning
Emission inventory
Global budget
Ozone depletion

ABSTRACT

Methyl halides (CH_3Cl, CH_3Br, and CH_3I) are ozone-depleting substances. Biomass burning (BB) is an important source of methyl halides. The temporal variations and global spatial distribution of BB methyl halide emissions are unclear. Thus, global methyl halide emissions from BB during 2003–2021 were estimated based on satellite data. A significant decreasing trend ($p < 0.01$) in global methyl halide emissions from BB was found between 2003 and 2021, with CH_3Cl emissions decreasing from 302 to 220 Gg yr^{-1}, CH_3Br emissions decreasing from 16.5 to 11.7 Gg yr^{-1}, and CH_3I emissions decreasing from 8.9 to 6.1 Gg yr^{-1}. From a latitudinal perspective, the northern high-latitude region (60–90° N) was the only latitude zone with significant increases in BB methyl halide emissions ($p < 0.01$). Based on an analysis of the drivers of BB methyl halide emissions, emissions from cropland, grassland, and shrubland fires were more correlated with the burned area, while BB emissions from forest fires were more correlated with the emissions per unit burned area. The non-BB emissions of CH_3Cl increased from 4749 Gg yr^{-1} in 2003 to 4882 Gg yr^{-1} in 2020, while those of CH_3Br decreased from 136 Gg yr^{-1} in 2003 to 118 Gg yr^{-1} in 2020 (global total CH_3I emissions are not available). The finding indicates that global CH_3Cl and CH_3Br emissions from sources besides BB increased and decreased during 2003–2020. Based on our findings, not only searching for unknown sources is important, but also re-evaluating known sources is necessary for addressing methyl halide emissions.

1. Introduction

Methyl halides (CH_3Cl, CH_3Br, and CH_3I) are ozone-depleting compounds. Notably, CH_3Cl is the largest source of Cl in the atmosphere, contributing 17% of the tropospheric Cl loading [1]; CH_3Br is the main source of stratospheric Br [1]; and CH_3I is an important short-lived halogenated substance (VSLS) [2]. The sources of methyl halides are abundant and are natural and anthropogenic [1,3]. CH_3Cl and CH_3I are mainly derived from natural sources and are not controlled under the Montreal Protocol (MP). Tropical and subtropical plants are the largest sources of global CH_3Cl emissions (4000–5000 Gg yr^{-1} (gigagrams per year, 1 Gg = 10^9 g)), which accounts for almost half of the global total CH_3Cl emissions [4]. Oceans emit 224 Gg yr^{-1} of CH_3I, accounting for 85% of the total global CH_3I emissions [5]; the remaining CH_3I emissions (~16 Gg yr^{-1}) are derived from rice paddies, biomass burning (BB), wetlands, etc. [6]. In contrast to other ODSs (chlorofluorocarbons and hydrochlorofluorocarbons) controlled under the MP, CH_3Br has abundant natural sources, mainly oceans (~40 Gg yr^{-1}) [3]. Currently, the sources are smaller than the sinks of CH_3Cl and CH_3Br worldwide, with gaps of 748 Gg yr^{-1} for CH_3Cl [2] and 15–17 Gg yr^{-1} for CH_3Br in 2018 [7]. Based on a recent study, 670 Gg yr^{-1} of CH_3Cl is emitted by tropical plants [4], which is 1370 Gg yr^{-1} lower than previous results [2]. Under this condition, the gap between the sources and sinks of CH_3Cl is 2118 Gg yr^{-1}, which is markedly larger than the previous gap of 748 Gg yr^{-1}. Therefore, re-evaluating the emissions from known sources could improve our understanding of the gaps between sources and sinks.

BB is a common natural emission source of the three methyl

* Corresponding author. College of Environmental & Resource Sciences, Zhejiang University, Hangzhou, Zhejiang, 310058, PR China.
E-mail address: fangxuekun@zju.edu.cn (X. Fang).

https://doi.org/10.1016/j.ese.2022.100228

halides [8,9]. In fact, BB emissions of CH_3Cl, CH_3Br, and CH_3I account for 9.7% [2], 20.2% [2], and 3.0% [6] of their global emissions, respectively. According to Nicewonger et al. and Yvon-Lewis et al. [7,10], BB is a key factor in explaining the interannual variability of atmospheric CH_3Br mole fractions during the EI Niño Southern Oscillation (ENSO). Thus, CH_3Br emissions from BB play a non-negligible role in the total CH_3Br emissions.

Currently, several approaches are available for estimating BB emissions, including the bottom-up emission ratio method [8,9], bottom-up satellite-derived burned area (BA) method [11,12], bottom-up satellite-derived fire radiative power (FRP) method [13–16], and top-down inversion method using atmospheric mole fraction observations and global transport models [6,17]. The estimates for BB CH_3Cl emissions markedly vary among studies, especially those using different approaches. Xiao et al. used the inversion method and estimated BB CH_3Cl emissions of 917 ± 198 Gg yr^{-1}, which accounts for 22 ± 5% of the global total CH_3Cl emissions [17]. By using the satellite-derived BA method, BB CH_3Cl emissions were estimated at 355 (142–569) Gg yr^{-1} [2], which were significantly lower than that reported by Xiao et al. [17]. Compared to CH_3Cl, the estimated gaps in the BB CH_3Br and CH_3I emissions were lower. The global BB CH_3Br and CH_3I emission values were approximately 10–50 and 1.6–8.0 Gg yr^{-1}, respectively [2,8,9]. Most of the previous studies, for example, Andreae et al. and Blake et al. [8,9] used CO or CO_2 as the tracer gas, measured the ratio of methyl halides to CO (or CO_2) in the local BB smoke, and calculated the target methyl halide emissions using the emission ratio and tracer emissions. However, this method may introduce great uncertainties in extrapolation from the local BB of a single biomass-burning type to the globe. Therefore, global BB CH_3Br and CH_3I emissions must be assessed using other methods, such as the satellite-derived FRP method.

Previous studies on BB methyl halide emissions rarely provided the spatial-temporal variation of emissions on a long-term scale. BB not only includes prescribed fires, such as human-planned ignition for landscape and agriculture management purposes, but also wildfires, such as forest, grassland, and savanna fires [18]. Human factors, such as land use and artificial ignition, have been linked to BB methyl halide emissions [19]. Frequent wildfires may lead to increased emissions of methyl halides [20,21]. Therefore, combined with variations in prescribed fires and wildfires, global BB methyl halide emissions may change in both time and space in the long term, which requires a comprehensive investigation.

In this study, satellite-derived burned dry matter mass (DM) data were employed to construct a high spatial resolution (0.05° × 0.05°) global BB emission inventory of CH_3Cl, CH_3Br, and CH_3I. The temporal trends and spatial distribution of global BB methyl halide emissions were analyzed, and the most important emission regions were identified. Our results on long-term-scale global emissions and detailed spatial distribution information are useful for further understanding the variations in BB emissions of methyl halides. Further implications of BB emissions for non-BB source emissions and the global budget were also presented in this study.

2. Methods and data

2.1. Calculating BB methyl halide emissions

The global BB emissions of three methyl halides (CH_3Cl, CH_3Br, and CH_3I) during 2003–2021 at a spatial resolution of 0.05° × 0.05° were estimated. The emissions for each methyl halide were calculated by multiplying the DM by the corresponding emission factor for each land-use type. The FRP method was developed owing to the introduction of fire observations in the MODIS era [13,14]. As a representative of the FRP method, the GFASv1.2 database (https://apps.ecmwf.int/datasets/data/cams-gfas/, last accessed on April 10, 2022) operates within the Copernicus Atmosphere Monitoring Service (CAMS) project and provides global daily average FRP, burnt dry matter, and BB emissions of 41 species. The GFASv1.2 database was extensively used in recent BB studies [22,23]. Herein, dry matter data from the GFASv1.2 database were employed to construct the BB methyl halide emission inventory. The emissions of methyl halides from BB were calculated as follows:

$$Emis_{s,i,j} = DM_{i,j} \times Area_{i,j} \times EF_{s,i,j} \quad (1)$$

where $DM_{i,j}$ is the DM combustion rate (kg m^{-2} s^{-1}), $Area_{i,j}$ is the area (m^2) of the (i, j) grid, $EF_{s,i,j}$ are the emission factors (g kg^{-1}) of sth species in the (i, j) grid, and $Emis_{s,i,j}$ is the BB emission (kg s^{-1}) of the sth species in the (i, j) grid. The accuracy of the above products used in this study has been validated [14]. However, note that since BB is only one emission source of methyl halides, our emission estimates are not directly validated by their global atmospheric observations.

2.2. Classifying the latitudes and biomass types

As the same biomass may have different emission factors at different latitudes [24], the latitudes were divided into six latitude zonal bands, similar to that performed in a previous study [7], including northern low-latitude (0°–30° N), northern mid-latitude (30°–60° N), northern high-latitude (60°–90° N), southern low-latitude (0°–30° S), southern mid-latitude (30°–60° S), and southern high-latitude (60°–90° S). To calculate the gridded emission factors, biomass was divided into six types according to Andreae [24]: boreal forest (60°–90° N and 60°–90° S), temperate forest (30°–60° N and 30°–60° S), tropical forest (0°–30° N and 0°–30° S), grassland, shrubland, and cropland (Table 1).

2.3. Generating gridded emission factors

In this study, globally gridded BB emission factors were generated for CH_3Cl, CH_3Br, and CH_3I at a spatial resolution of 0.05° × 0.05°. The emission factors of each grid were determined based on the corresponding biomass type [24]. Further, the biomass type of each grid was determined based on the grid's land-use type and latitude. Thereafter, the emission factors of the grid were derived. By traversing the annual land-use type matrix and assigning the emission factor of each grid, the emission factor matrix for the current year can be generated.

Global land-use type data from 2003 to 2020 were obtained from the MODIS satellite-derived product, MCD12C1 (https://ladsweb.modaps.eosdis.nasa.gov/archive/allData/6/MCD12C1/, last accessed on March 25, 2022), which provides global annual gridded land-use type data at a spatial resolution of 0.05° × 0.05°. Of note, as data for 2021 are currently unavailable in this product, we assumed there was no significant change in 2021 compared to 2020 and used the 2020 land-use type data as a replacement for 2021. In the MCD12C1 product, the global land-use types were divided into 17 categories based on the International Geosphere-Biosphere Programme (IGBP) classification standard, as shown in Table 1. For land-use types without BB (e.g., urban and built-up lands), the emission factors were set to 0. For the land-use type with BB, the land-use type was found to correspond with the above six biomass types (see Table 1). The emission factors for each type of flammable biomass were derived from Andreae [24]. The emission factors corresponding to each land-use type are summarized in Table 1. Note that Andreae [24] did not distinguish emission factors by types of forests (evergreen needleleaf forests, evergreen broadleaf

Table 1
Emission factors (g kg^{-1}) of each land-use type and biomass type for CH_3Cl, CH_3Br, and CH_3I.

Land-use type	Biomass type	CH_3Cl	CH_3Br	CH_3I
Water bodies	–	0	0	0
Forests	Boreal Forest	0.06	0.0029	0.0004
	Temperate forest	0.042	0.0015	0.0005
	Tropical forest	0.029	0.0078	0.0068
Closed shrublands	Shrublands	0.063	0.0027	0.0007
Open shrublands				
Woody savannas	Grassland	0.063	0.0027	0.0007
Savannas				
Grasslands				
Permanent wetlands	–	0	0	0
Croplands	Cropland	0.17	0.0011	0.0002
Cropland/natural vegetation mosaics				
Urban and built-up Lands	–	0	0	0
Permanent snow and ice	–	0	0	0
Barren	–	0	0	0

"-" indicates that the land-use type has no biomass covered.

forests, deciduous needleleaf forests, deciduous broadleaf forests, and mixed forests).

2.4. Calculating global top-down emissions with a one-box model

To estimate the changes in non-BB methyl halide emissions, a one-box model and global annual mean mole fractions of CH_3Cl and CH_3Br (note that there were no CH_3I observation data) from AGAGE (https://agage.mit.edu/, last accessed on June 20, 2022) were employed to calculate the top-down emissions of CH_3Cl and CH_3Br. The following formulas were for the one-box model [25].

$$\frac{dC_{i,j}}{dt} = F_i \times E_{i,j} - \frac{C_{i,j}}{\tau_i} \quad (2)$$

Equation (2) can be transformed into equation (3):

$$E_{i,j} = \frac{\frac{dC_{i,j}}{dt} + \frac{C_{i,j}}{\tau_i}}{F_i} \quad (3)$$

where $C_{i,j}$ is the mole fraction (ppt; parts per trillion) of substance i in year j, $E_{i,j}$ is the annual emissions (kg yr^{-1}; kilogram per year) of substance i in year j, τ_i is the lifetime (years) of substance i, and F_i is a factor linking the emissions to the global mole fractions (ppt kg^{-1}).

$$F_i = \left(\frac{N_A}{N_a}\right)\frac{F_{surf}}{M_i} = 5.68 \times 10^{-9}\frac{F_{surf}}{M_i} \quad (4)$$

where M_i is the molecular weight (kg mol^{-1}) of the substance i, N_A is the Avogadro number, N_a is the number of global atmospheric molecules, and F_{surf} is a factor that links the global mean surface mole fractions to the global mean atmospheric mixing ratios (1.07 is used in this study for methyl halides) [1].

3. Results and discussion

3.1. Temporal and spatial variations of emissions

In this study, the global emissions and corresponding CFC-11-equivalent emissions of three methyl halides (CH_3Cl, CH_3Br, and CH_3I) from BB were estimated during 2003–2021. The corresponding CFC-11-eq emissions were equal to the emissions of these three methyl halides multiplied by the corresponding ODP values (0.015 for CH_3Cl, 0.57 for CH_3Br, and 0.017 for CH_3I) [2]. Fig. 1 shows the time series of global BB methyl halide emissions and the corresponding CFC-11-eq emissions during 2003–2021. The global average annual BB emission of CH_3Cl was 249 Gg yr^{-1} (3.7 Gg yr^{-1} CFC-11-eq), while that of CH_3Br was 14 Gg yr^{-1} (7.8 Gg yr^{-1} CFC-11-eq), and that of CH_3I was 7.2 Gg yr^{-1} (0.12 Gg yr^{-1} CFC-11-eq).

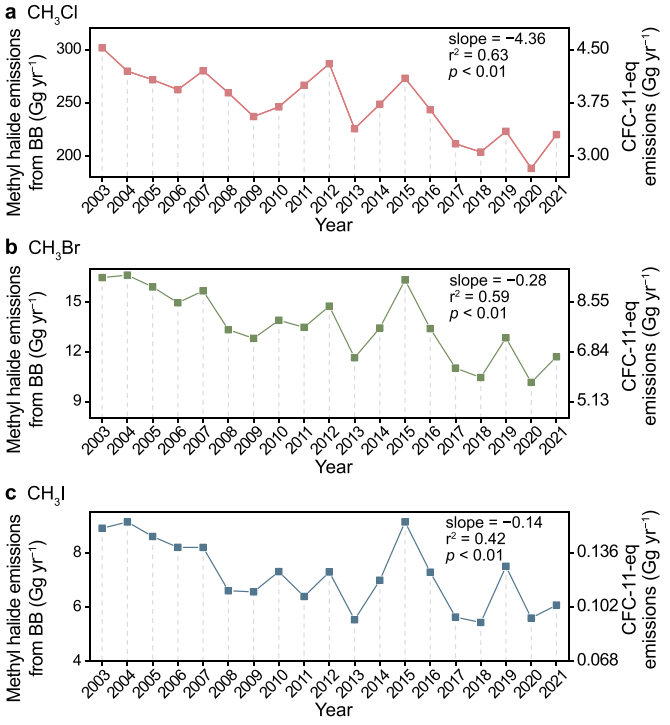

Fig. 1. Time series of global BB methyl halide emissions and CFC-11-eq emissions during 2003–2021: **a**, CH_3Cl; **b**, CH_3Br; **c**, CH_3I.

The global methyl halide emissions from BB displayed a downward trend in general ($p < 0.01$), from 302 Gg yr^{-1} CH_3Cl, 16.5 Gg yr^{-1} CH_3Br, and 8.9 Gg yr^{-1} CH_3I in 2003 to 220 Gg yr^{-1} CH_3Cl, 11.7 Gg yr^{-1} CH_3Br, and 6.1 Gg yr^{-1} CH_3I in 2021. Although the general trend of emissions displayed this declining trend, increases were recorded in individual years, such as 2009–2012 and 2013–2015 (Fig. 1), which reflects the randomness of BB to some extent. BB is affected by various factors, such as climatic conditions and human activities [26]. Drought and temperature changes caused by ENSO exacerbate the occurrence of global fires [7], resulting in increased CH_3Br emissions from BB during certain

years. As shown in Fig. 2, the boreal frigid zone was identified as the only latitude zone whose BB methyl halide emissions generally increased ($p < 0.01$) during 2003–2021. As shown in Fig. 2f, the proportion of BB methyl halide emissions from the boreal frigid zone to the total global emissions increased to 14% by 2021. In particular, BB methyl halide emissions from the boreal frigid zone increased from 0.28 Gg yr^{-1} CFC-11-eq in 2015 to 1.4 Gg yr^{-1} CFC-11-eq in 2021. The boreal frigid zone has been warming twice as fast as the whole globe [27], which has led to the rapid green-up of vegetation in North America and Eurasia [28], providing more fuel for BB. The water content of combustible biomass significantly decreases with climate warming, which indicates that the possibility of wildfires increases in the boreal frigid zone [29].

Herein, the changes in the global spatial distribution and the top ten emitter countries of BB methyl halides were presented (Figs. 3 and 4). As shown in Fig. 3, global BB methyl halide emissions presented spatial heterogeneity, and some regions were identified as emission hotspots, including central South Africa, South America, northern Australia, southeastern Russia, northwestern Canada, and southeast Asia. From the perspective of latitude, the tropical zone (0–30° S and 0–30° N) contributed the largest emissions, with an average annual methyl halide emission of 192 Gg yr^{-1} CH_3Cl, 12 Gg yr^{-1} CH_3Br, and 5.9 Gg yr^{-1} CH_3I during 2003–2021, followed by the temperate zone (30–60° S and 30–60° N), with an average annual methyl halide emission of 44 Gg yr^{-1} CH_3Cl, 1.5 Gg yr^{-1} CH_3Br, and 1.1 Gg yr^{-1} CH_3I. The boreal frigid zone (60–90° N) contributed the smallest BB methyl halide emissions, with an annual average of 12 Gg yr^{-1} CH_3Cl, 0.54 Gg yr^{-1} CH_3Br, and 0.14 Gg yr^{-1} CH_3I. Fig. 4 shows the top ten emission countries (ranked by average values of CFC-11-eq emissions during 2003–2005 and 2019–2021) and their corresponding continents. Although the BB methyl halide emissions of nearly all countries have decreased, Russia's BB methyl halide emissions have increased from 1.08 Gg yr^{-1} CFC-11-eq between 2003 and 2005 to 1.18 Gg yr^{-1} CFC-11-eq between 2019 and 2021. Russia also ranked first globally in terms of BB methyl halide emissions between 2019 and 2021.

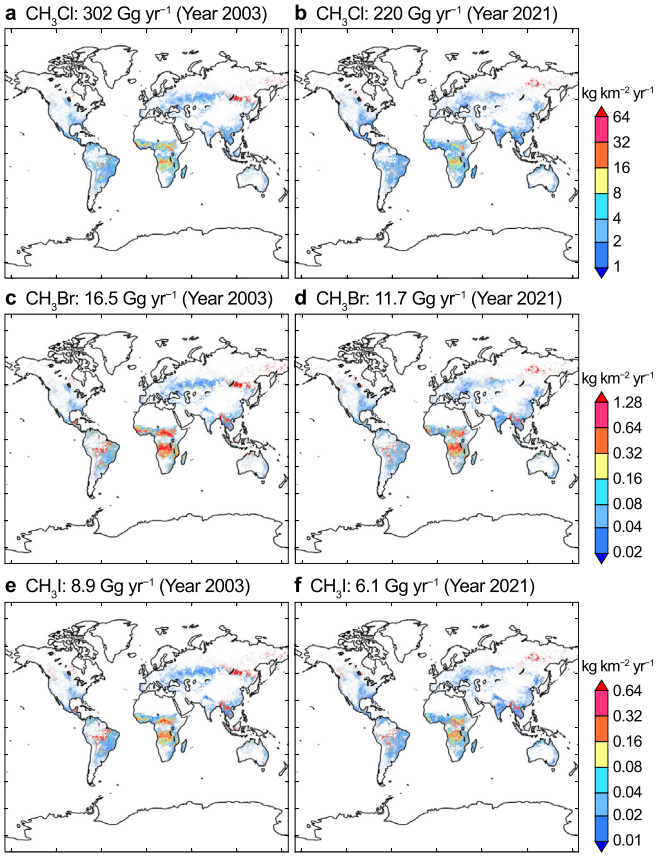

Fig. 3. Global spatial distribution of BB methyl halide emissions in 2003 and 2021: **a**, CH_3Cl (Year 2003); **b**, CH_3Cl (Year 2021); **c**, CH_3Br (Year 2003); **d**, CH_3Br (Year 2021); **e**, CH_3I (Year 2003); **f**, CH_3I (Year 2021).

3.2. Change in emissions by land-use type

The impact factors of global BB emissions are complex, and include fire weather, fuel availability, land-use change, and man-made ignition [29,30]. Global BB emissions increased during 1700–1900, peaked in the 1910s, and then began to decrease, and that land-use change is the main driver of the decrease in global BB emissions since the 1910s [31]. Herein, the global area during

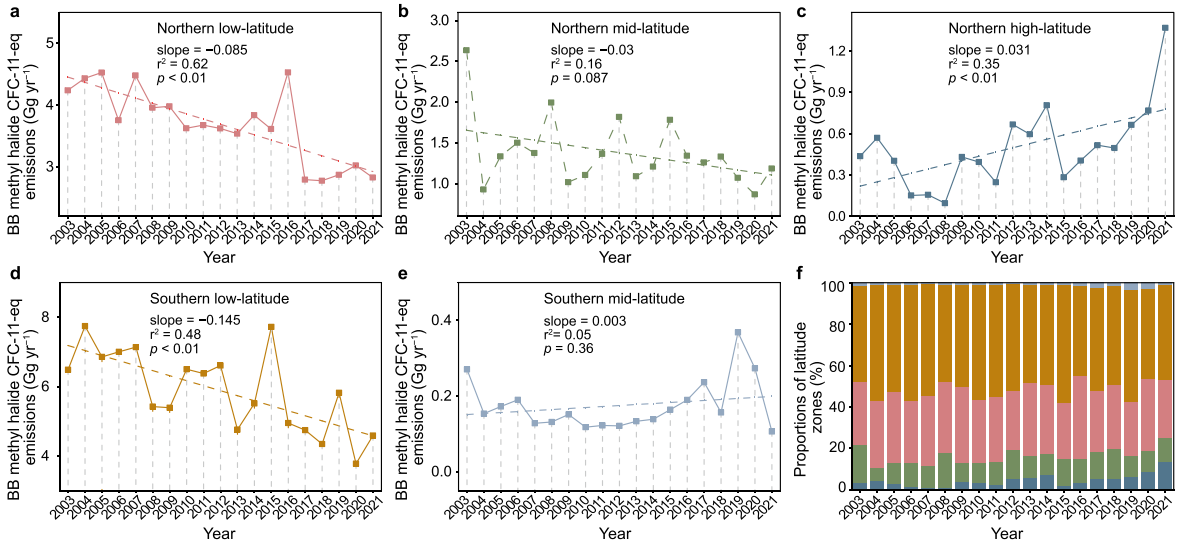

Fig. 2. Time series of different latitude zones (tropical, temperate, and boreal frigid) for BB methyl halide emissions during 2003–2021: **a**, northern low-latitude; **b**, northern mid-latitude; **c**, northern high-latitude; **d**, southern low-latitude; **e**, southern mid-latitude; **f**, proportions of latitude zones (%).

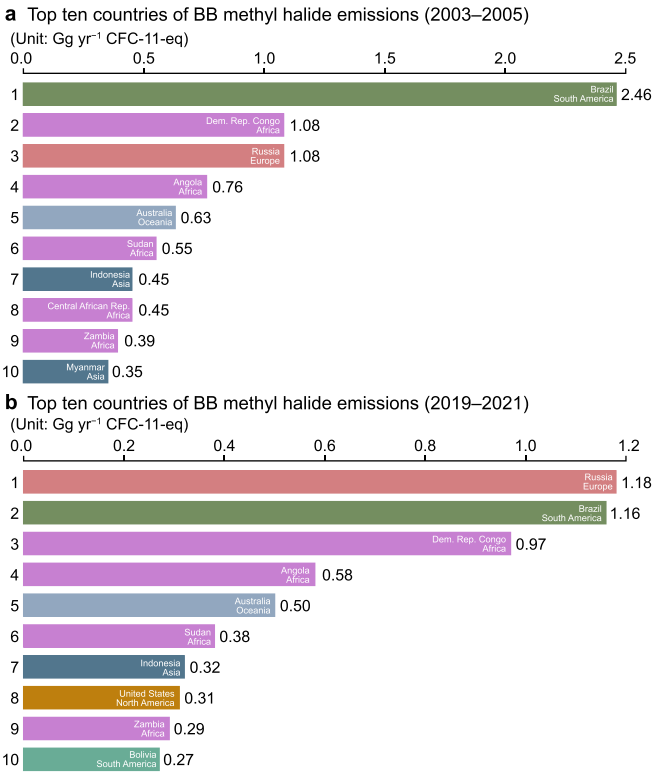

Fig. 4. Changes in the top ten emitter countries of BB methyl halide emissions from 2003 to 2005 (**a**) to 2019–2021 (**b**). The different colors of the bars represent different continents that those countries are located in (e.g., the purple represents Africa).

2003–2020 was obtained from the MCD12C1 product of MODIS (https://ladsweb.modaps.eosdis.nasa.gov/archive/allData/6/MCD12C1/) and burned areas during 2003–2016 for the forest area, cropland area, grassland area, and shrubland area were obtained from the GFED4s database (https://www.geo.vu.nl/~gwerf/GFED/GFED4/, last accessed on July 14, 2022). As shown in Fig. 5, the global forest area decreased by 36 Mha (1 Mha = 10^6 ha = 10^4 km^2), and BB methyl halide emissions from forest decreased by 7.0 Gg yr^{-1} CH_3Cl, 2.4 Gg yr^{-1} CH_3Br, and 1.9 Gg yr^{-1} CH_3I. The global cropland, grassland, and shrubland areas increased by 23, 29, and 10 Mha, respectively, from 2003–2005 to 2019–2020. Agricultural expansion is the main driver of the decrease in the global forest area, especially tropical forests in Africa [32]. Agricultural expansion has led to a reduction in global BB [33]. Besides, as shown in Fig. 5, BB methyl halide emissions decreased by 13.2 Gg yr^{-1} CH_3Cl, 0.09 Gg yr^{-1} CH_3Br, and 0.02 Gg yr^{-1} CH_3I from cropland; 53.6 Gg yr^{-1} CH_3Cl, 2.3 Gg yr^{-1} CH_3Br, 0.6 Gg yr^{-1} CH_3I from grassland; and 0.03 Gg yr^{-1} CH_3Cl from shrubland (the decrease in CH_3Br and CH_3I emissions could be ignored). The increasing cropland, grassland, and shrubland areas did not increase the corresponding BB methyl halide emissions.

As shown in Fig. 6, the correlation (Pearson's $r = 0.950$) of BB methyl halide emissions from forest fires with emissions per unit burned forest area is stronger than the correlation (Pearson's $r = 0.692$) of BB methyl halide emissions from forest fires with the global burned forest area. Therefore, compared with the burned forest area, the combustion intensity per unit burned area plays a more important role in global forest fire emissions. To some extent, this conclusion is consistent with that of Zheng et al. [34], who reported that global forest fire emissions display a trend that differs from the trend of global burned area, indicating that burned area is

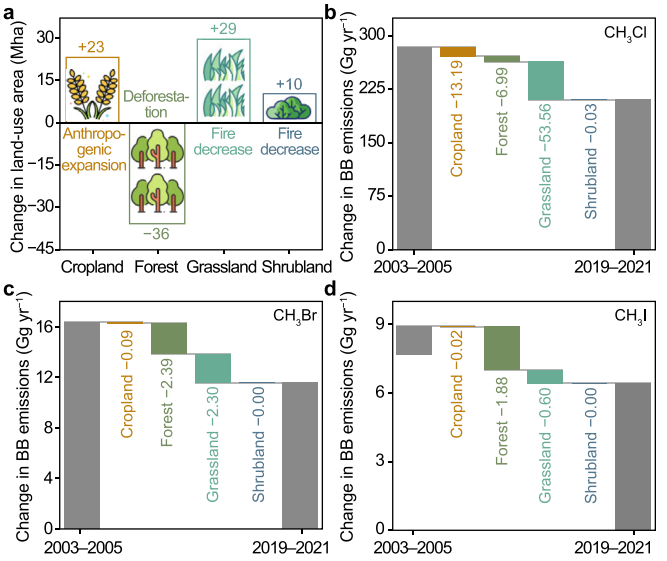

Fig. 5. Change in land-use areas from 2003–2005 to 2019–2020 (**a**) and changes in BB methyl halide emissions by land-use type from 2003–2005 to 2019–2021 (**b**, CH_3Cl; **c**, CH_3Br; **d**, CH_3I). The emissions and areas are presented as average values for 2003–2005 and 2019–2021 (or 2019–2020).

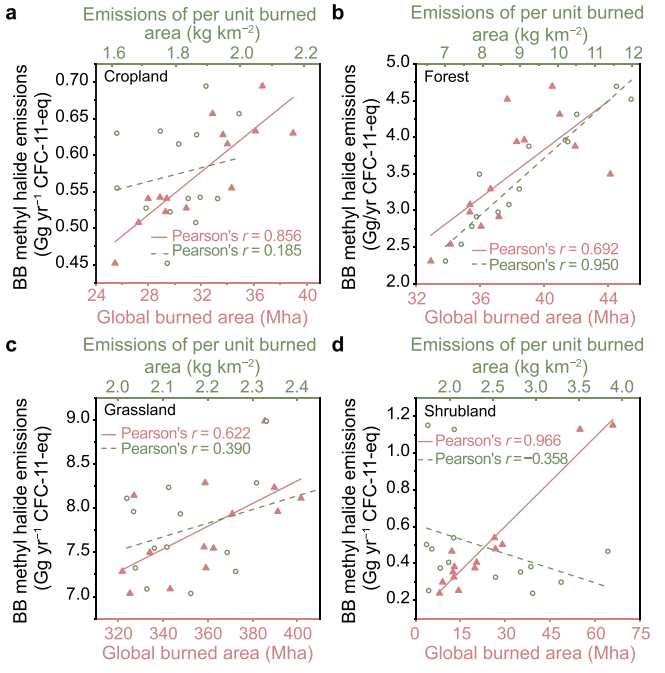

Fig. 6. Correlations of BB methyl halide emissions with global burned area and emissions per unit burned area by land-use type from 2003 to 2016: **a**, cropland; **b**, forest; **c**, grassland; **d**, shrubland. The pink solid triangles and pink solid lines indicate the correlations of BB methyl halide emissions with global burned area. The green hollow circles and green dotted lines indicate the correlations of BB methyl halide emissions with emissions per unit burned area.

not a dominant factor of forest fire emissions. Accordingly, other factors, such as combustion intensity per unit burned area, may have a greater influence on forest fire emissions. In contrast to forest fire emissions, BB methyl halide emissions from cropland, grassland, and shrubland fires might be more correlated with the global burned area of the corresponding biomass types (Fig. 6). The aboveground biomass loading per unit area of these three biomass

types was smaller than that of the forest. As a result, their combustion completeness was greater than that of forest fires. Overall, compared to the emissions per unit burned area, the global burned area of these three biomass types is a dominant factor in their BB methyl halide emissions.

3.3. Comparison with previous studies

As shown in Fig. 7, we compared the BB emissions of CH_3Cl, CH_3Br, and CH_3I obtained in this study with those obtained in other studies. Considering the different years of this study and previous studies [8,9,35], we linearly extrapolated BB methyl halide emissions during 2003–2021 to 1990–2002 (Fig. 7). The decreasing trend obtained by linear regression is consistent with the trend of global BB emissions [26,31], which verifies the reasonability of our linear extrapolation. As shown in Fig. 7, the extrapolated BB CH_3Cl emissions are 345 Gg yr^{-1} in 1990 and 336 Gg yr^{-1} in 1992, which are still significantly lower than the results of 910 Gg yr^{-1} in 1990 by Lobert et al. [35], 1100 Gg yr^{-1} in 1992 by Andrea et al. [8], and 900 Gg yr^{-1} in 1992 by Blake et al. [9]. These researchers used the emission ratio method to calculate global BB CH_3Cl emissions by extrapolating the emission ratios in a local fire of a single biomass type (such as a forest fire in Africa) to the globe. Under this extrapolation, the emission ratios of different biomass types and latitudes were set to be the same, enabling the extrapolation to introduce large biases or uncertainties. The emission ratios of different biomass types in different regions of the world vary significantly (Fig. 8). The CH_3Br/CO_2 emission ratio of tropical forests was almost five-fold higher than that of temperate forests. For example, previous studies [36,37] used the emission ratio method and estimated the BB CH_3Cl emissions 611 ± 38 and 515 (226–904) Gg yr^{-1} lower than those of studies used the same method [8,9,35]. The such finding indicates that the estimates were markedly affected by the emission ratio used in the study.

Our estimates of CH_3Br are consistent in magnitude with those of Nicewonger et al. [7], who estimated global annual BB CH_3Br emissions using dry matter burnt data from the GFED4s dataset and emission factors from Andreae [24]; however, few differences were found in the temporal trend (Pearson's r = 0.706, Fig. S1). The decreasing trend in this study is more significant than that in the study by Nicewonger et al. [7], with linear regression slopes of −0.28 and −0.11 Gg yr^{-1}, respectively. The differences between this study and that of Nicewonger et al. [7] were derived from burned dry mass matter calculated using the two databases (GFED4s and GFASv1.2) and the emission factor matrix generated by the land cover product. To explore the key factor leading to the differences in this study and Nicewonger et al. [7], we calculated global BB CH_3Br emissions with DM from the GFED4s dataset and analyzed the correlations of BB CH_3Br emissions in this study (DM from GFASv1.2), this study (DM from GFED4s), and Nicewonger et al. [7] (DM from GFED4s). As

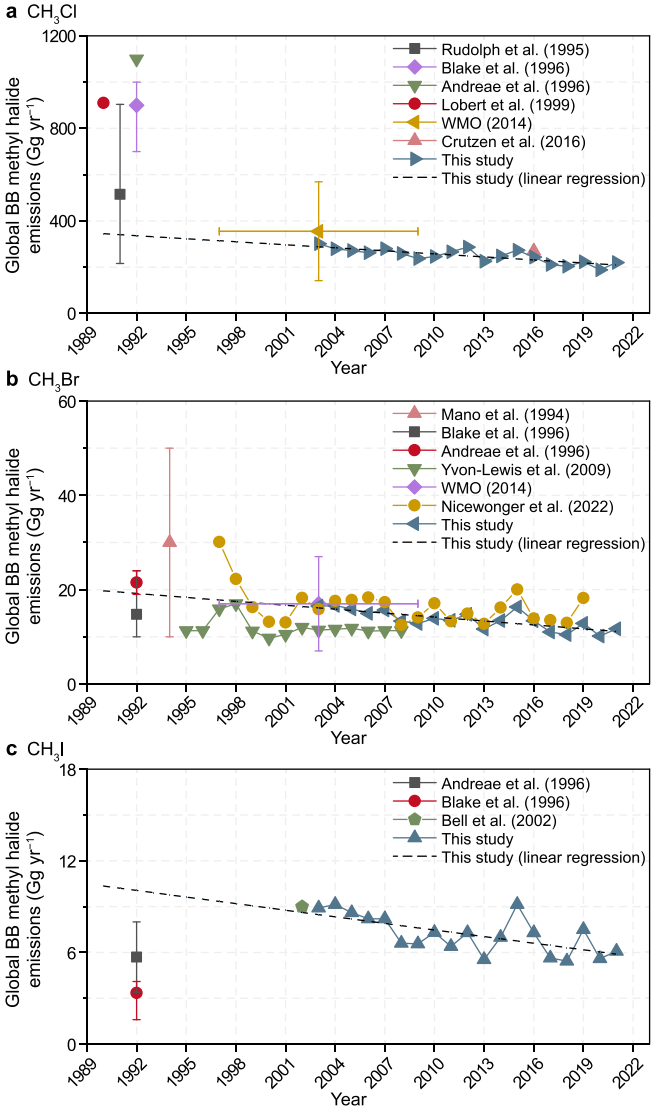

Fig. 7. Comparison of the present study estimates with previous estimates: **a**, CH_3Cl; **b**, CH_3Br; **c**, CH_3I. The blue solid triangles represent this study, and the black dotted lines represent the estimates using linear regression extrapolation.

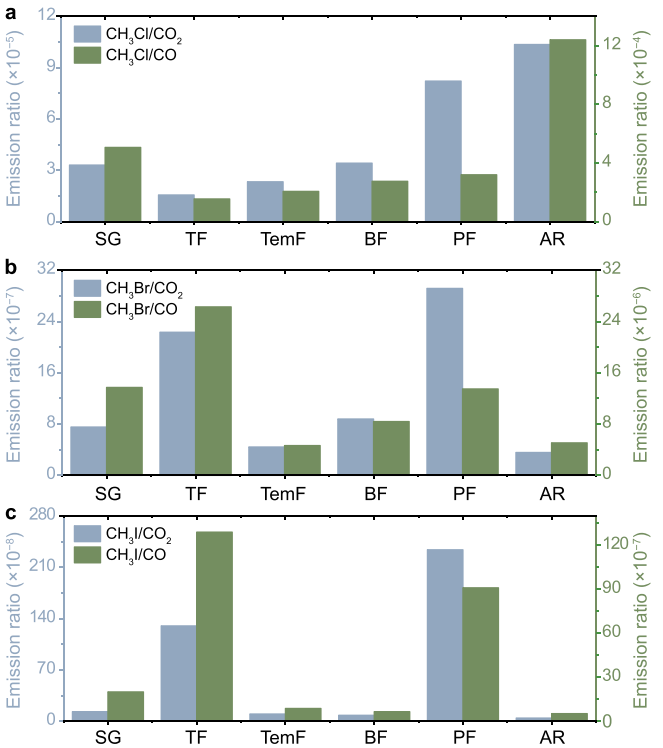

Fig. 8. Emission ratios of CH_3Cl (**a**), CH_3Br (**b**), and CH_3I (**c**) relative to CO_2 or CO from different biomass types, calculated by Andrea [24]. "SG" represents savanna and grassland, "TF" represents tropical forest, "TemF" represents temperate forest, "BF" represents boreal forest, "PF" represents peat fire, and "AR" represents agricultural residue.

shown in Fig. S1, the correlation (Pearson's r value) between this study (DM from GFASv1.2) and this study (DM from GFED4s) is 0.687, which is weaker than that of 0.928 between this study (DM from GFED4s) and Nicewonger et al. [7] (DM from GFED4s). Therefore, burned dry mass matter calculated by GFASv1.2 and GFED4s datasets rather than the emission factors matrix is the key factor leading to the different emission estimates in this study (DM from GFASv1.2) and Nicewonger et al. [7]. Good correlations were found between BB methyl halide emissions in this study and BB CO_2, CO, CH_4, and total particulate matter (TPM) emissions in the GFED4s and GFASv1.2 databases (Table 2 and Fig. S2), aligning with the co-emission of these gases during BB.

3.4. Implications for global and regional budget

To explore the changes in the global methyl halide budget throughout the study period, the non-BB emissions were equal to global total emissions minus BB emissions. Due to that bottom-up estimates for the latest year are not available [2], and top-down estimates have been updated to the 2020 year using a one-box model (Table S2), we adopted top-down estimates for the global total methyl halide emissions. Our top-down estimate of CH_3Cl emissions is 5001 Gg yr^{-1} on average during 2003–2020, which is close to 4715 Gg yr^{-1} on average estimated using the stable carbon isotope ratios method by Keppler et al. [38]. To some extent, this can validate our top-down emission estimates using a one-box model. As shown in Fig. 9a, non-BB CH_3Cl emissions increased from 4749 Gg yr^{-1} in 2003 to 4882 Gg yr^{-1} in 2021. Therefore, more attention should be paid to non-BB sources of CH_3Cl, including known sources and potential new sources. Bahlmann et al. [4] reported that CH_3Cl emissions from tropical plants were overestimated by 1370 Gg yr^{-1}. Under these conditions, the global sink and source gap of CH_3Cl will be 2118 Gg yr^{-1} instead of the value of 748 Gg yr^{-1} reported by WMO [2]. Besides, a new CH_3Cl emission source was discussed by Jiao et al. [39], who found that the use of pesticides based on Cu^{2+} resulted in CH_3Cl emissions via an abiotic pathway from soil and seawater. Re-evaluating emissions from known sources and finding new sources are thus necessary to improve our understanding of the global CH_3Cl budget.

On a regional scale, our BB CH_3Br emission estimation is helpful for reducing the gap between top-down and bottom-up estimates. Choi et al. [40] reported a nearly 2.9 Gg yr^{-1} emissions gap between top-down emissions and bottom-up emissions in China. Furthermore, these researchers calculated 1.5 Gg yr^{-1} of unreported emissions, including rapeseed, agricultural residue burning, and agricultural harvest treatments, leaving 1.4 Gg yr^{-1} to be fully attributed to China's illegal emissions. In addition to agricultural residue burning, forest burning, grassland burning, and shrubland burning are BB sources of CH_3Br [24]. Herein, the CH_3Br emission of

Table 2
Correlation analysis of CH_3Cl, CH_3Br, and CH_3I emissions in this study with CO, CO_2, CH_4, and TPM in the GFED4s and GFASv1.3 database.

Substance (database)	CH_3Cl (This study)		CH_3Br (This study)		CH_3I (This study)	
	r	p_value	r	p_value	r	p_value
CO (GFAS1.3)	0.73	0.003	0.87	0.000	0.86	0.000
CO (GFED4)	0.54	0.048	0.79	0.001	0.84	0.000
CO_2 (GFAS1.3)	0.90	0.000	0.92	0.000	0.82	0.000
CO_2 (GFED4)	0.67	0.009	0.91	0.000	0.92	0.000
CH_4 (GFAS1.3)	0.77	0.001	0.95	0.000	0.96	0.000
CH_4 (GFED4)	0.31	0.286	0.58	0.029	0.67	0.009
TPM (GFAS1.3)	0.94	0.000	0.93	0.000	0.85	0.000
TPM (GFED4)	0.67	0.009	0.88	0.000	0.90	0.000

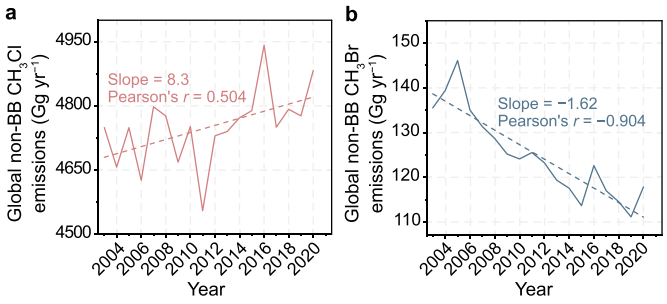

Fig. 9. Top-down and non-BB emissions of CH_3Cl (**a**) and CH_3Br (**b**) during 2003–2021. The solid pink and dotted blue lines represent the linear regression results of non-BB CH_3Cl and CH_3Br emissions, respectively.

all BB types in China was 0.15 Gg yr^{-1} (average for 2008–2019), which is 0.08 Gg yr^{-1} higher than the value of 0.07 Gg yr^{-1} reported by Choi et al. [40] (only agricultural residue burning emissions). Therefore, if emissions from these three BB types are added, the gap between the top-down and bottom-up estimates is less than 1.4 Gg yr^{-1}.

4. Conclusions

In this study, we estimated the global BB emissions of CH_3Cl, CH_3Br, and CH_3I during 2003–2021 based on satellite-derived burnt dry matter data from the GFASv1.2 database. The global BB methyl halide emissions generally declined from 302 Gg yr^{-1} CH_3Cl, 16.5 Gg yr^{-1} CH_3Br, and 8.9 Gg yr^{-1} CH_3I in 2003 to 220 Gg yr^{-1} CH_3Cl, 11.7 Gg yr^{-1} CH_3Br, and 6.1 Gg yr^{-1} CH_3I in 2021. The boreal frigid zone was the only latitude zone whose BB methyl halide emissions increased (from 11.0 Gg yr^{-1} CH_3Cl, 0.47 Gg yr^{-1} CH_3Br, and 0.12 Gg yr^{-1} CH_3I in 2003 to 34.4 Gg yr^{-1} CH_3Cl, 1.48 Gg yr^{-1} CH_3Br, and 0.37 Gg yr^{-1} CH_3I in 2021). The global spatial distribution of BB methyl halide emissions revealed obvious spatial heterogeneity. Central South Africa, South America, northern Australia, southeastern Russia, northwestern Canada, and Southeast Asia were the six emission hotspots. BB methyl halide emissions from all four biomass types declined from 2003 to 2021. Furthermore, for cropland, grassland, and shrubland, the global burned area may be the dominant driver (Pearson's r values are 0.856, 0.622, and 0.966, respectively) of their BB methyl halide emissions; however, the emissions per unit burned area may be the main driver (Pearson's r value is 0.950) of BB methyl halide emissions in forests. Overall, this study improves the current understanding of the temporal variation and spatial distribution of global BB methyl halide emissions. Further, non-BB emissions of CH_3Cl were found to increase from 4749 Gg yr^{-1} in 2003 to 4882 Gg yr^{-1} in 2021, implying that further research should focus on non-BB emission studies, and include a search for new emission sources and better estimates of known sources.

Declaration of competing interest

The authors declare that they have no known competing financial interests or personal relationships that could have appeared to influence the work reported in this paper.

Acknowledgments

This work was supported by the National Key Research and Development Program of China (2019YFC0214503), the Ecological Civilization Project of Zhejiang University, Key R&D Program of

Zhejiang Province (2022C03154), Fundamental Research Funds for the Central Universities (2020QNA6015), and National Natural Science Foundation of China (2210060183). We acknowledge the Emissions of Atmospheric Compounds and Compilation of Ancillary Data (https://eccad.aeris-data.fr/essd-surf-emis-cams-bio/) for archiving the emission inventory data of CAMS-GLOB-BIO; the Level-1 and Atmosphere Archive & Distribution System (LAADS) Distributed Active Archive Center (DAAC) (https://ladsweb.modaps.eosdis.nasa.gov/archive/allData/6/MCD12C1/) for archiving the global land cover data of MCD12C1; the Copernicus Atmosphere Monitoring Service (https://apps.ecmwf.int/datasets/data/cams-gfas/) for archiving the global gridded dry matter burnt data of the GFASv1.2 database; and the AGAGE (https://agage.mit.edu/data) for archiving the global annual mean concentration data of atmospheric CH_3Cl and CH_3Br.

Appendix A. Supplementary data

Supplementary data to this article can be found online at https://doi.org/10.1016/j.ese.2022.100228.

References

[1] World Meteorological Organization (WMO), Scientific Assessment of Ozone Depletion: 2018 Executive Summary, 2018.
[2] World Meteorological Organization (WMO), Scientific Assessment of Ozone Depletion, 2014, 2014.
[3] E.S. Saltzman, M.R. Nicewonger, S.A. Montzka, S.A. Yvon Lewis, A post-phaseout retrospective reassessment of the global methyl bromide budget, J. Geophys. Res. Atmos. 127 (2022).
[4] E. Bahlmann, F. Keppler, J. Wittmer, M. Greule, H.F. Schöler, R. Seifert, C. Zetzsch, Evidence for a major missing source in the global chloromethane budget from stable carbon isotopes, Atmos. Chem. Phys. 19 (2019) 1703–1719.
[5] J. Zhang, D.J. Wuebbles, D.E. Kinnison, A. Saiz Lopez, Revising the ozone depletion potentials metric for short-lived chemicals such as CF3I and CH_3I, J. Geophys. Res. Atmos. 125 (2020).
[6] N. Bell, L. Hsu, D.J. Jacob, M.G. Schultz, D.R. Blake, J.H. Butler, D.B. King, J.M. Lobert, E. Maier-Reimer, Methyl iodide: atmospheric budget and use as a tracer of marine convection in global models, J. Geophys. Res. Atmos. 107 (2002) 1–8.
[7] M.R. Nicewonger, E.S. Saltzman, S.A. Montzka, ENSO-driven fires cause large interannual variability in the naturally emitted, ozone-depleting trace gas CH_3Br, Geophys. Res. Lett. 49 (2022).
[8] M.O. Andreae, E. Atlas, G.W. Harris, G. Helas, A. De Kock, R. Koppmann, M. Welling, Methyl halides emissions from savanna fires in southern Africa, J. Geophys. Res. Atmos. 101 (1996) 23603–23613.
[9] N.J. Blake, D.R. Blake, B.C. Sive, T.Y. Chen, F.S. Rowland, J.E. Collins Jr., B.E. Anderson, Biomass burning emissions and vertical distribution of atmospheric methyl halides and other reduced carbon gases in the South Atlantic region, J. Geophys. Res. Atmos. 101 (1996) 24151–24164.
[10] S.A. Yvon-Lewis, E.S. Saltzman, S.A. Montzka, Recent trends in atmospheric methyl bromide: analysis of post-Montreal Protocol variability, Atmos. Chem. Phys. 9 (2009) 5963–5974.
[11] J.T. Randerson, Y. Chen, G.R. van der Werf, B.M. Rogers, D.C. Morton, Global burned area and biomass burning emissions from small fires, J. Geophys. Res. 117 (2012) G4012.
[12] L. Giglio, J.T. Randerson, G.R. van der Werf, Analysis of daily, monthly, and annual burned area using the fourth-generation global fire emissions database (GFED4), J. Geophys. Res.: Biogeosciences 118 (2013) 317–328.
[13] M.J. Wooster, G. Roberts, G.L.W. Perry, Y.J. Kaufman, Retrieval of biomass combustion rates and totals from fire radiative power observations: FRP derivation and calibration relationships between biomass consumption and fire radiative energy release, J. Geophys. Res. 110 (2005).
[14] J.W. Kaiser, A. Heil, M.O. Andreae, A. Benedetti, N. Chubarova, L. Jones, J.J. Morcrette, M. Razinger, M.G. Schultz, M. Suttie, G.R. van der Werf, Biomass burning emissions estimated with a global fire assimilation system based on observed fire radiative power, Biogeosciences 9 (2012) 527–554.
[15] L. Yin, P. Du, M. Zhang, M. Liu, T. Xu, Y. Song, Estimation of emissions from biomass burning in China (2003–2017) based on MODIS fire radiative energy data, Biogeosciences 16 (2019) 1629–1640.
[16] X. Pan, C. Ichoku, M. Chin, H. Bian, A. Darmenov, P. Colarco, L. Ellison, T. Kucsera, A. Da Silva, J. Wang, T. Oda, G. Cui, Six global biomass burning emission datasets: intercomparison and application in one global aerosol model, Atmos. Chem. Phys. 20 (2020) 969–994.
[17] X. Xiao, R.G. Prinn, P.J. Fraser, P.G. Simmonds, R.F. Weiss, S. O'Doherty, B.R. Miller, P.K. Salameh, C.M. Harth, P.B. Krummel, L.W. Porter, J. Mühle, B.R. Greally, D. Cunnold, R. Wang, S.A. Montzka, J.W. Elkins, G.S. Dutton, T.M. Thompson, J.H. Butler, B.D. Hall, S. Reimann, M.K. Vollmer, F. Stordal, C. Lunder, M. Maione, J. Arduini, Y. Yokouchi, Optimal estimation of the surface fluxes of methyl chloride using a 3-D global chemical transport model, Atmos. Chem. Phys. 10 (2010) 5515–5533.
[18] R. Pavlovic, J. Chen, K. Anderson, M.D. Moran, P.A. Beaulieu, D. Davignon, S. Cousineau, The FireWork air quality forecast system with near-real-time biomass burning emissions: recent developments and evaluation of performance for the 2015 North American wildfire season, J. Air Waste Manag. Assoc. 66 (2016) 819–841.
[19] D.M.J.S. Bowman, G.J. Williamson, J.T. Abatzoglou, C.A. Kolden, M.A. Cochrane, A.M.S. Smith, Human exposure and sensitivity to globally extreme wildfire events, Nat. Ecol. Evol. 1 (2017).
[20] E. Chuvieco, L. Giglio, C. Justice, Global characterization of fire activity: toward defining fire regimes from Earth observation data, Global Change Biol. 14 (2008) 1488–1502.
[21] M.S. Balshi, A.D. Mcguire, P. Duffy, M. Flannigan, J. Walsh, J. Melillo, Assessing the response of area burned to changing climate in western boreal North America using a Multivariate Adaptive Regression Splines (MARS) approach, Global Change Biol. 15 (2009) 578–600.
[22] C.L. Reddington, L. Conibear, S. Robinson, C. Knote, S.R. Arnold, D.V. Spracklen, Air pollution from forest and vegetation fires in Southeast Asia disproportionately impacts the poor, GeoHealth 5 (2021).
[23] I.R. van der Velde, G.R. van der Werf, S. Houweling, J.D. Maasakkers, T. Borsdorff, J. Landgraf, P. Tol, T.A. van Kempen, R. van Hees, R. Hoogeveen, J.P. Veefkind, I. Aben, Vast CO2 release from Australian fires in 2019-2020 constrained by satellite, Nature 597 (2021) 366–369.
[24] M.O. Andreae, Emission of trace gases and aerosols from biomass burning – an updated assessment, Atmos. Chem. Phys. 19 (2019) 8523–8546.
[25] X. Fang, B.R. Miller, S. Su, J. Wu, J. Zhang, J. Hu, Historical emissions of HFC-23 (CHF3) in China and projections upon policy options by 2050, Environ. Sci. Technol. 48 (2014) 4056–4062.
[26] C. Wu, S. Sitch, C. Huntingford, L.M. Mercado, S. Venevsky, G. Lasslop, S. Archibald, A.C. Staver, Reduced global fire activity due to human demography slows global warming by enhanced land carbon uptake, Proc. Natl. Acad. Sci. USA 119 (2022).
[27] M. Hisano, M. Ryo, X. Chen, H.Y.H. Chen, Rapid functional shifts across high latitude forests over the last 65 years, Global Change Biol. 27 (2021) 3846–3858.
[28] H. Park, S. Jeong, J. Peñuelas, Accelerated rate of vegetation green-up related to warming at northern high latitudes, Global Change Biol. 26 (2020) 6190–6202.
[29] X.J. Walker, B.M. Rogers, S. Veraverbeke, J.F. Johnstone, J.L. Baltzer, K. Barrett, L. Bourgeau-Chavez, N.J. Day, W.J. de Groot, C.M. Dieleman, S. Goetz, E. Hoy, L.K. Jenkins, E.S. Kane, M.A. Parisien, S. Potter, E.A.G. Schuur, M. Turetsky, E. Whitman, M.C. Mack, Fuel availability not fire weather controls boreal wildfire severity and carbon emissions, Nat. Clim. Change 10 (2020) 1130–1136.
[30] C. Molinari, V. Lehsten, O. Blarquez, C. Carcaillet, B.A.S. Davis, J.O. Kaplan, J. Clear, R.H.W. Bradshaw, The climate, the fuel and the land use: long-term regional variability of biomass burning in boreal forests, Global Change Biol. 24 (2018) 4929–4945.
[31] D.S. Ward, E. Shevliakova, S. Malyshev, S. Rabin, Trends and variability of global fire emissions due to historical anthropogenic activities, Global Biogeochem. Cycles 32 (2018) 122–142.
[32] Y. Feng, Z. Zeng, T.D. Searchinger, A.D. Ziegler, J. Wu, D. Wang, X. He, P.R. Elsen, P. Ciais, R. Xu, Z. Guo, L. Peng, Y. Tao, D.V. Spracklen, J. Holden, X. Liu, Y. Zheng, P. Xu, J. Chen, X. Jiang, X. Song, V. Lakshmi, E.F. Wood, C. Zheng, Doubling of annual forest carbon loss over the tropics during the early twenty-first century, Nat. Sustain. 5 (2022) 444–451.
[33] Z. Kovacic, O. Viteri Salazar, The lose - lose predicament of deforestation through subsistence farming: unpacking agricultural expansion in the Ecuadorian Amazon, J. Rural Stud. 51 (2017) 105–114.
[34] B. Zheng, P. Ciais, F. Chevallier, E. Chuvieco, Y. Chen, H. Yang, Increasing forest fire emissions despite the decline in global burned area, Sci. Adv. 7 (2021) h2646.
[35] J.M. Lobert, W.C.L.J. Keene, R. Yevich, Global chlorine emissions from biomass burning: reactive chlorine emissions inventory, J. Geophys. Res. Atmos. D7 (1999) 8373–8389.
[36] Y. Yoshida, Y. Wang, T. Zeng, A three-dimensional global model study of atmospheric methyl chloride budget and distributions, J. Geophys. Res. 109 (2004), D24309.
[37] J. Rudolph, A. Khedim, R. Koppmann, Field study of the emissions of methyl chloride and other halocarbons from biomass burning in western Africa, J. Atmos. Chem. 22 (1995) 67–80.
[38] F. Keppler, D.B. Harper, T. Röckmann, R.M. Moore, J.T.G. Hamilton, New insight into the atmospheric chloromethane budget gained using stable carbon isotope ratios, Atmos. Chem. Phys. 5 (2005) 2403–2411.
[39] Y. Jiao, W. Zhang, J.Y.R. Kim, M.J. Deventer, J. Vollering, R.C. Rhew, Application of copper(II)-based chemicals induces CH_3Br and CH_3Cl emissions from soil and seawater, Nat. Commun. 13 (2022).
[40] H. Choi, M. Park, P.J. Fraser, H. Park, S. Geum, J. Mühle, J. Kim, I. Porter, P.K. Salameh, C.M. Harth, B.L. Dunse, P.B. Krummel, R.F. Weiss, S. O'Doherty, D. Young, S. Park, Top-down and bottom-up estimates of anthropogenic methyl bromide emissions from eastern China, Atmos. Chem. Phys. 22 (2022) 5157–5173.